

## Supporting Information

### **Boosted Interfacial Charge Transfer in SnO<sub>2</sub>/SnSe<sub>2</sub> Heterostructures: Toward Ultrasensitive Room-temperature H<sub>2</sub>S Detection**

Tingting Wang,<sup>a</sup> You Wang,<sup>\*a,b</sup> Quan Sun,<sup>b</sup> Shengliang Zheng,<sup>b</sup> Lizhao Liu,<sup>\*c</sup> Jialu Li,<sup>d</sup> and Juanyuan Hao<sup>\*b</sup>

a. School of Chemistry and Chemical Engineering, Harbin Institute of Technology, Harbin 150001, China. E-mail: y-wang@hit.edu.cn

b. School of Materials Science and Engineering, Harbin Institute of Technology, Harbin 150001, China. E-mail: jyhao@hit.edu.cn; y-wang@hit.edu.cn

c. Key Laboratory of Materials Modification by Laser, Ion and Electron Beams (Ministry of Education), Dalian University of Technology, Dalian 116024, China. E-mail: lizhao\_liu@dlut.edu.cn

d. College of Chemistry, Jilin University, Changchun 130012, China

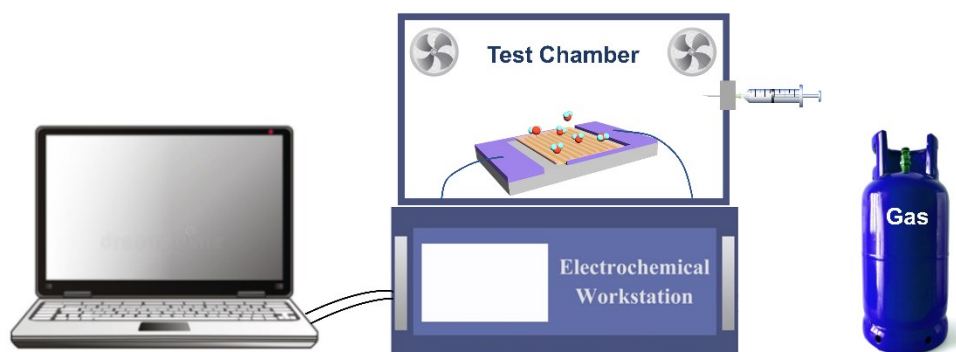


**Fig. S1** Schematic diagram of the sensor measurement.

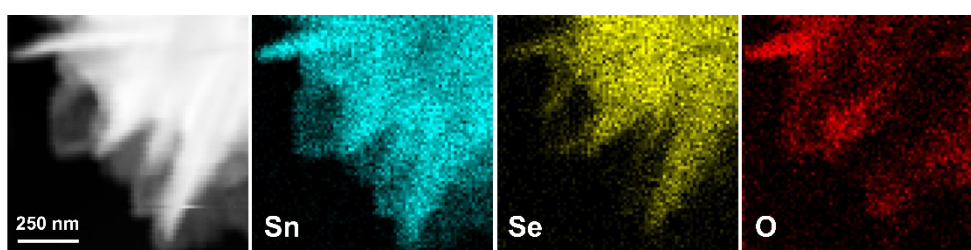


**Fig. S2** EDX elemental mapping of SnO<sub>2</sub>/SnSe<sub>2</sub>-4h.

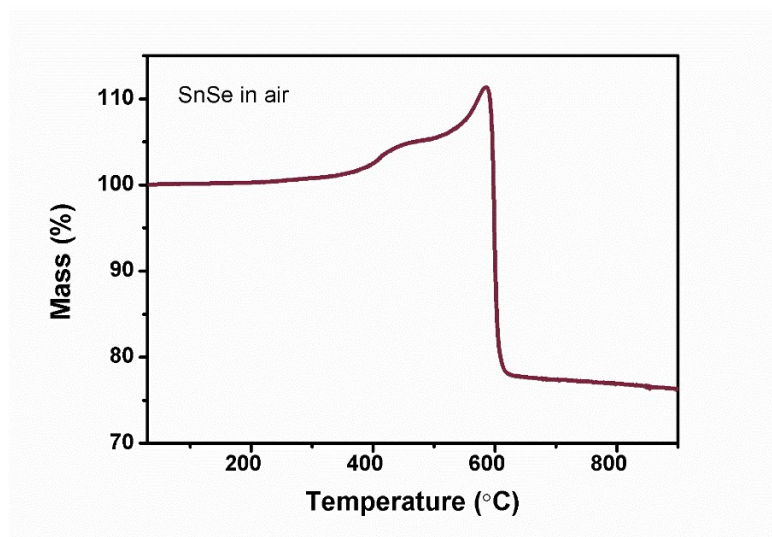


**Fig. S3** TGA curves of SnSe from room temperature to 900 °C in air.

As can be seen from Fig. S3, a weight gain process between 400 to 600 °C along with a significant weight loss around 600 °C are observed. The weight change is the combination of weight gain due to oxygen pickup from air to form the oxides and weight loss due to sublimation of Se and Se-containing oxides.

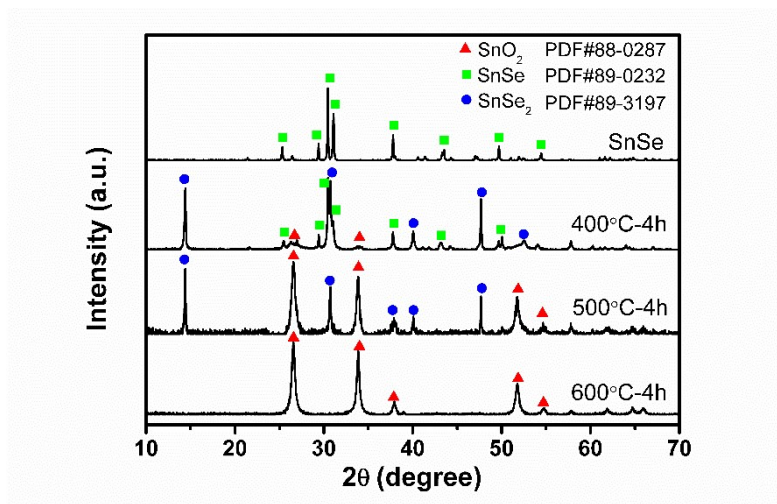


**Fig. S4** XRD patterns of pristine SnSe and the obtained samples after thermal oxidation at 400 °C, 500 °C, and 600 °C for 4 h.

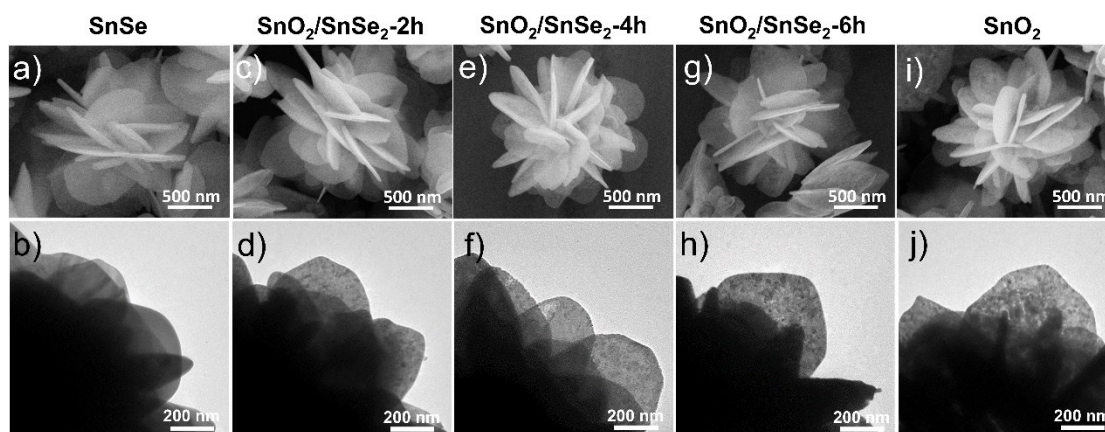


**Fig. S5** SEM and TEM images of (a, b) pristine SnSe, (c, d) SnO<sub>2</sub>/SnSe<sub>2</sub>-2h, (e, f) SnO<sub>2</sub>/SnSe<sub>2</sub>-4h, (g, h) SnO<sub>2</sub>/SnSe<sub>2</sub>-6h, (i, j) SnO<sub>2</sub>.

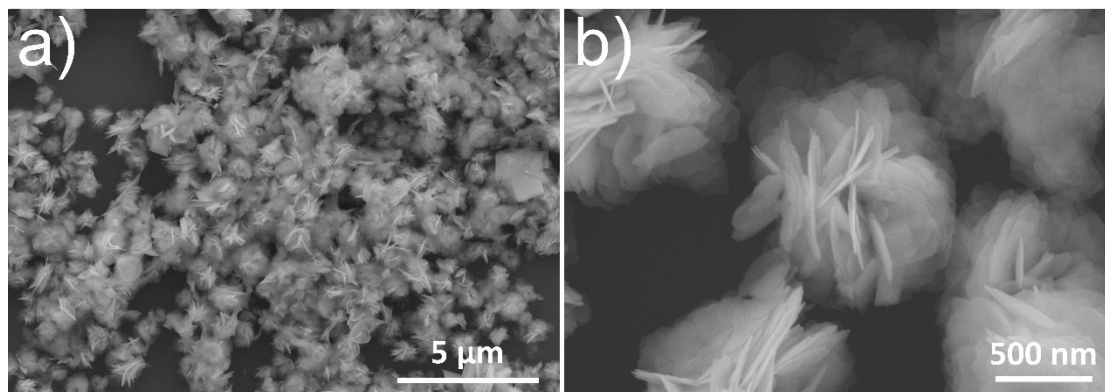


**Fig. S6** (a, b) SEM images of pristine SnSe<sub>2</sub>.

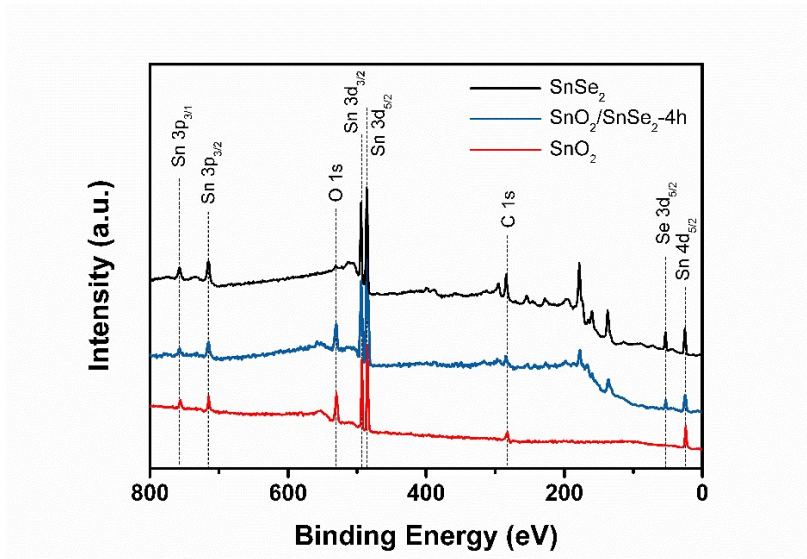


**Fig. S7** The survey XPS curves of SnSe<sub>2</sub>, SnO<sub>2</sub>/SnSe<sub>2</sub>-4h, and SnO<sub>2</sub>.

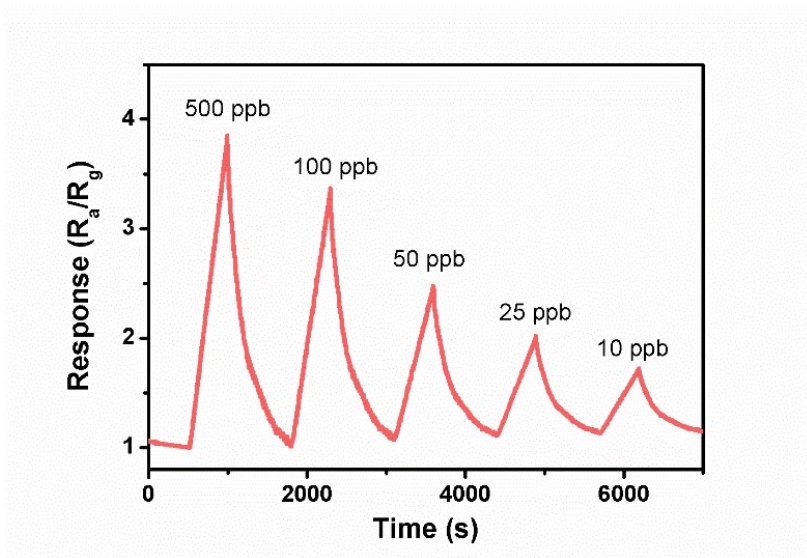


**Fig. S8** Dynamic response of the SnO<sub>2</sub>/SnSe<sub>2</sub>-4h sensor with ppb-level H<sub>2</sub>S concentrations ranging from 500 to 10 ppb.

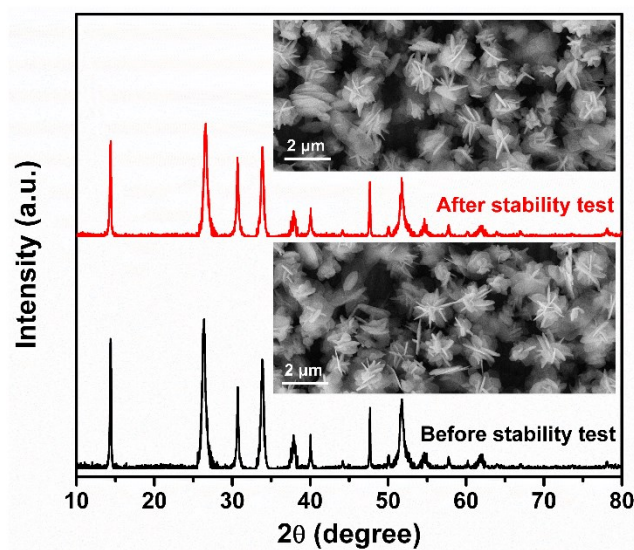


**Fig. S9** XRD patterns and SEM images of SnO<sub>2</sub>/SnSe<sub>2</sub> sensing materials before and after the stability test.

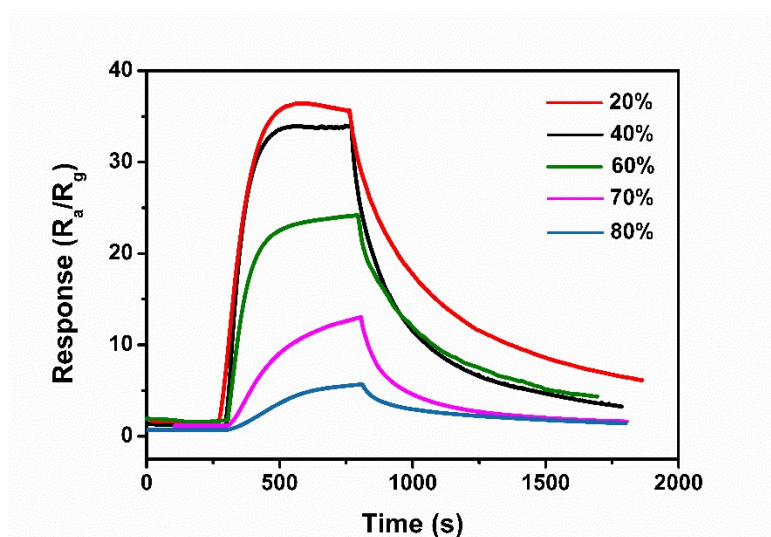


**Fig. S10** The sensing behavior of SnO<sub>2</sub>/SnSe<sub>2</sub>-4h sensor to 10 ppm H<sub>2</sub>S in different humidity at room-temperature.

A commercial damp-heat chamber (CK-80G, Kingjo) was used to control the relative humidity (RH) during the sensing test. The result shows a decrease in sensing response toward 10 ppm H<sub>2</sub>S from 37 to 5 with the increase of RH from 20 to 80%. The possible reason for this phenomenon is that the adsorption of water molecules may occupy a part of active sites for the attraction of target gas. Besides, water molecules would prevent the adsorption of oxygen molecules in the high-humidity environment, which leads to

a lower adsorption concentration of ionized oxygen involved in the sensing reaction, and thus a decreased sensing response. [1-3]

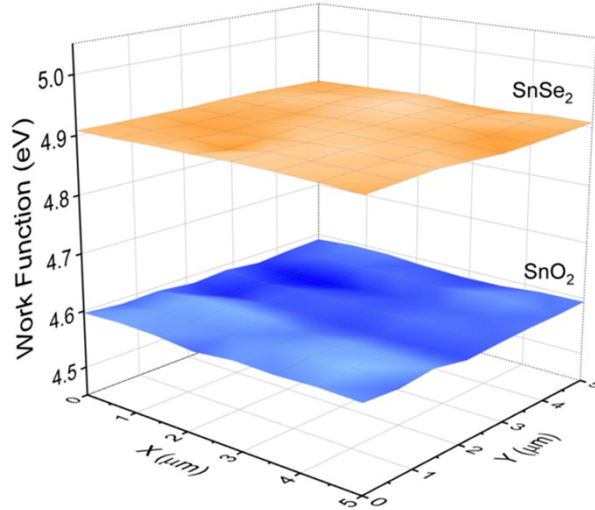


**Fig. S11** Work functions of SnSe<sub>2</sub> (4.9 eV) and SnO<sub>2</sub> (4.6 eV) measured by the Kelvin probe based on 256 data points.

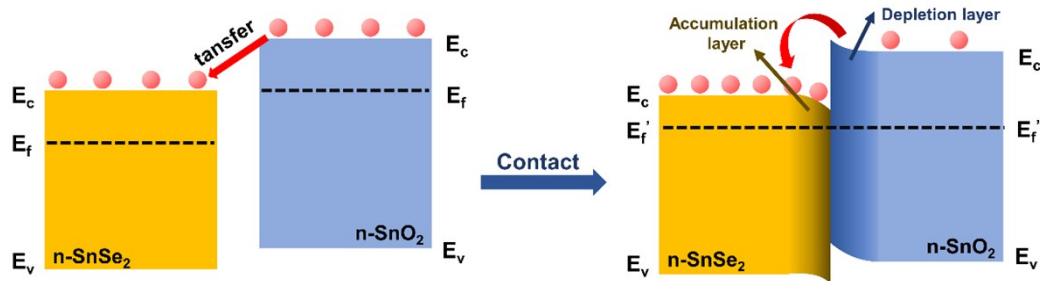


**Fig. S12** The schematic and band diagrams of SnO<sub>2</sub>/SnSe<sub>2</sub> heterostructures before and after equilibrium ( $E_c$  = conduction band edge energy;  $E_v$  = valence band edge energy;  $E_f$  = Fermi level).

As SnO<sub>2</sub> has a higher Fermi energy level than that of SnSe<sub>2</sub>, the electrons will transfer from SnO<sub>2</sub> to SnSe<sub>2</sub> and form an interface depletion layer at SnO<sub>2</sub> as well as an accumulation layer at SnSe<sub>2</sub> when the SnO<sub>2</sub>/SnSe<sub>2</sub> heterojunction is formed.

## References

- [1]. L. Liu, Y. Wang, Y. Dai, G. Li, S. Wang, T. Li, T. Zhang and S. Qin, In Situ Growth of NiO@SnO<sub>2</sub> Hierarchical Nanostructures for High Performance H<sub>2</sub>S Sensing, *ACS Appl. Mater. Interfaces*, 2019, **11**, 44829-44836.
- [2]. B. Y. Song, M. Zhang, Y. Teng, X. F. Zhang, Z. P. Deng, L. H. Huo and S. Gao, Highly selective ppb-level H<sub>2</sub>S sensor for spendable detection of exhaled biomarker and pork freshness at low temperature: Mesoporous SnO<sub>2</sub> hierarchical architectures derived from waste scallion root, *Sens. Actuators, B*, 2020, **307**, 127662.
- [3]. A. Mirzaei, S. S. Kim and H. W. Kim, Resistance-based H<sub>2</sub>S gas sensors using metal oxide nanostructures: A review of recent advances, *J Hazard. Mater.*, 2018, **357**, 314-331.